Hydrol. Earth Syst. Sci. Discuss., 7, 3189–3211, 2010
www.hydrol-earth-syst-sci-discuss.net/7/3189/2010/
doi:10.5194/hessd-7-3189-2010

Hydrology and Earth System Sciences Discussions

Simulation of snow distribution and melt under cloudy conditions in an alpine watershed

H.-Y. Li and J. Wang

Cold and Arid Regions Environmental and Engineering Research Institute, Chinese Academy of Sciences, Lanzhou 730000, China

Received: 30 March 2010 – Accepted: 14 May 2010 – Published: 27 May 2010

Correspondence to: H.-Y. Li (lihongyi@lzb.ac.cn)

Published by Copernicus Publications on behalf of the European Geosciences Union.

Abstract

An energy balance method and remote sensing data were used to simulate snow distribution and melt in an alpine watershed in Northwestern China within a complete snow accumulation-melt period. Spatial energy budgets were simulated using the meteorological observations and digital elevation model of the watershed. A linear interpolation method was used to discriminate daily snow cover area under cloudy conditions, using Moderate Resolution Imaging Spectroradiometer data. Hourly snow distribution and melt, snow cover extent, and daily discharge were included in the simulated results. The bias error between field snow water equivalent samplings and simulated results is −2.1 cm, and Root Mean Square Error is 33.9 cm. The Nash and Sutcliffe efficiency statistic (R^2) between measured and simulated discharges is 0.673, and the volume difference (Dv) is 3.9%. Using the method introduced in this article, modeling spatial snow distribution and melt runoff will become relatively convenient.

1 Introduction

Snow is a very important component of the climate system because of its significant effect on surface energy and water balance; thus, its accurate representation is essential to a better understanding of climate effects on the hydrological cycle (Tarboton et al., 2000). Rather than using difficult field measurements, Remote Sensing (RS) is now more widely used in modeling snow because of its unique advantages in obtaining large-scale ground information (Seidel and Martinec, 2004). Snow cover area (SCA) with higher spatial resolution could be obtained through RS of near-infrared and visible wavelengths (Hall et al., 2006). Then SWE distribution could be simulated by the combination of energy balance method and SCA data (Cline et al., 1998). Because spatial and temporal variation of snow is fundamentally driven by the energy and mass balance, thus SWE change in a complete snow accumulation-melt period could be

HESSD

7, 3189–3211, 2010

regarded as the function of snow duration (T) and energy input (E).

$$\Delta \mathrm{SWE} = f(E,T) \quad (1)$$

With continuous observation of SCA and accurate simulation of spatial distribution of energy budgets, snow duration (T) and energy input (E) for snowmelt at each grid could be obtained and snow processes could be theoretically calculated.

However, the key of this method is obtaining snow existence durations under cloudy conditions. Cline et al. (1998) had simulated the spatial energy balance and obtained the total SWE distribution by this method, but only a few satellite images were used. Snowfall, cloudy condition, and pre-snowmelt season were ignored in the simulation. The discrimination of snow existence under clouds is a known problem. For instance, the Moderate Resolution Imaging Spectroradiometer (MODIS) data which provide daily SCA information is used widely in mountainous SWE reconstruction, land surface model, and hydrological model (Zaitchik and Rodell, 2009; Parajka and Bloeschl, 2008; Durand et al., 2008), because of its high temporal and spatial resolution and accurate identification of snow. However, the main disadvantage of the MODIS sensor is that it is unable to record observations under cloud-covered regions (Gafurov and Bardossy, 2009). Thus, some researchers had to give up scenes affected seriously by clouds (Su et al., 2008), or use the eight-day composite maximum snow cover tile product as replacement (Tekeli et al., 2005). Abundant data were wasted because it was inconvenient to understand snow accumulation and melt processes accurately. In this paper, a linear interpolation method was developed to avoid the influence of clouds on SCA data and calculate SWE change utilizing MODIS data.

The goal of this paper is to model continuous SWE and melt runoff by an energy balance method under cloudy conditions in an alpine watershed. The method consists of three steps: (1) estimating daily snow existence using MODIS data and meteorological observation; (2) modeling daily spatial energy balance processes and calculating the total SWE distribution using the estimated SCA, Digital Elevation Model (DEM), and meteorological observation; and (3) calculating daily SWE distribution based on calculated hourly snowmelt and snowfall observation.

HESSD
7, 3189–3211, 2010

2 Data and observations

2.1 Site description

Binggou watershed, located in the upstream of Heihe river basin in Northwestern China, was chose as one of the foci experiment areas within the WATER (Watershed Allied Telemetry Experimental Research) framework (Li, 2009). The altitude range of Binggou watershed is from 3440 to 4400 m and the area is about 30.27 km^2, a seasonally snow-covered region. Mean depth of the seasonal snowpack is about 0.5 m, up to a maximum of 0.8–1.0 m. Snow redistribution is remarkable because of the interaction between blowing snow and complex terrain. There is more snowfall in spring and autumn than in winter. Snowfall period first takes place from November to April, rainy season from May to August, and snowfall comes again after September. Mean air temperature at an altitude of 3450 m was about −2.5 °C in the 2008 snow season; minimum temperature was −29.6 °C, and maximum was 19.9 °C.

Meteorological data were collected using two Automatic Weather Stations (AWS), Dadongshu Mountain Pass Snow Observation Station (DY) (4146.8 m, 100°14′ E, 38°01′ N) and Binggou Cold Region Meteorological Station (BG) (3449.4 m, 100°13′ E, 38°04′ N) (Fig. 1), during a complete snow accumulation-melt period from 1 November 2007 to 31 May 2008. A hydrological gauge was installed at the outlet of the watershed to measure daily discharge.

Snow characteristics data were collected through a series of field measurements in the snow season of 2008. These datasets include basic snow properties such as snow depth, density, grain size, temperature, emissivity, and so on. The topographic information such as elevation, slope and aspect of slope, were all resulted from the DEM of the Binggou watershed with 50 m resolution.

HESSD
7, 3189–3211, 2010

2.2 Discrimination of snow existence under cloudy conditions

MODIS snowcover products, MODIS/Terra Snow Cover Daily L3 Global 500 m Grid (MOD10A1), were collected. Version 005 of MOD10A1 contains a new fractional snowcover product developed from a linear fit of binary Thematic Mapper snowcover to the normalized difference snow index of MODIS (Painter et al., 2009). Data fields in MOD10A1 data, SCA, and Snow Cover Fraction (SCF), were used to model snow distribution. Resolution of the MODIS data was degraded from 500 to 50 m in order to match the DEM.

Spatial distribution of clouds is largely different between daily MOD10A1 scenes, while SCAs and snowpack positions changed relatively slowly. If a cloudy duration is short enough at a grid of the study area, then estimating snowcover fraction values of the grid accurately on cloudy days by interpolation of a series of cloudless SCF values of the grid is possible.

A simple linear method was used to obtain daily SCA in the study. Considering snowpack evolution at each grid of MOD10A1 scene, SCA depletion is continuous except when snowfall happens in each grid. Assuming a cloudy duration from 1 day to $n-1$ day, and 0 day and n day is cloudless, the SCF value of x day [SCF(t_x)] in this cloudy duration can be obtained by a linear interpolation method according to Eq. (2)

$$\mathrm{SCF}(t_x) = \frac{x}{n} \cdot (\mathrm{SCF}(t_n) - \mathrm{SCF}(t_0)) + \mathrm{SCF}(t_0) \quad (2)$$

Where SCF(t_0) is the SCF value of the 0 day, and SCF(t_n) is the SCF value of the n day.

3 Methods

A distributed physical snow model was designed to model daily snow distribution and melt. Meteorological data, MODIS snowcover data, and DEM were the major inputs for the model. Spatial meteorological elements were calculated using continuous hourly

HESSD
7, 3189–3211, 2010

meteorological observations and DEM of the watershed. Continuous SCF datasets were used to simulate daily snow ablation by a distributed energy balance method. Finally, total SWE change over the entire snow season was obtained. Daily snow distribution was calculated based on total SWE change, daily snowfall records, and calculated daily snowmelt.

3.1 Model description

3.1.1 Spatial SWE calculation

At the grid, SWE at t time (M_{grid}) is estimated from

$$M_{\text{grid}}(t) = M_{\text{grid}}(0) + \sum_{x=0}^{t} \left(P_x \cdot S - \left[R_{\text{grid}}(x) + E_{\text{grid}}(x) \right] \right) \quad (3)$$

where P is the snowfall water equivalent rate (m/s), S is the grid area (m^2), R_{grid} is the melt-water output (m^3/s) at the grid, and E_{grid} is the snowpack mass loss of sublimation (m^3/s). Assuming sublimation and melt are homogeneous in a grid,

$$R_{\text{grid}} = R \cdot \text{SCF} \cdot S \quad (4)$$

$$E_{\text{grid}} = E \cdot \text{SCF} \cdot S \quad (5)$$

where R is the melt runoff rate at the point (m/s), E is the snow sublimation rate (m/s), and SCF is the snow fraction proportion.

3.1.2 Energy balance method

The energy budget for the snowpack can be written as

$$Q_{\text{melt}} = S_{\text{net}} + L_{\text{net}} + H + LE + G + Q_{\text{p}} - Q_{\text{i}} \quad (6)$$

$$E = \frac{LE}{Lf} \quad (7)$$

HESSD
7, 3189–3211, 2010

where Q_{melt} is the energy budget for snowmelt outputs (J), and Q_i is the internal energy change of snowpack (J). S_{net}, L_{net}, H, LE, G, and Q_p are net shortwave radiant energy input (J), net longwave radiant input (J), sensible heat (J), latent heat of sublimation (J), ground heat conduction (J), and precipitation sensible and latent heat (J), respectively. Lf is the latent heat of fusion (J/kg).

Before melt runoff can be released from the snowpack, the average temperature of the snowpack must be raised to the melting point and its maximum liquid-water-retaining capacity must be reached. Further net energy inputs (Q_{melt}) produce melt-water outputs

$$R = \frac{Q_{melt}}{\rho_w L f B} \tag{8}$$

where ρ_w is the liquid water density (kg/m^3), and B is the thermal quality of the snow (0.97).

3.1.3 SWE adjustment with MODIS snowcover data

Snow existence is one of the necessary conditions of snowmelt occurrence. In modeling SWE, snow depth was also modeled for energy exchange computation at each time step. The modeled snow depth of a grid is possibly 0, but there is actually snow in the SCA image because of external factors such as blowing snow and internal errors of the model. In this case, SWE was estimated from SCF using an empirical method (Yang et al., 1997; Essery and Pomeroy, 2004),

$$\frac{M_{avg}}{M_{ini}} = \tanh\left(\frac{SCF}{C_s}\right) \tag{9}$$

where M_{avg} is the average SWE of the grid, M_{ini} is the pre-melt SWE of the grid, and C_s is the coefficient of variation. M_{ini} is assumed to be 20 cm and the C_s 0.95.

Since the snowpack is regarded as a single layer, an iterative algorithm that has been used in the UEB model (Tarboton, 1996) was used to model snow surface temperature.

HESSD
7, 3189–3211, 2010

First, the model was calibrated at the point scale at DY station without using RS data. The calibrated parameters are shown in Table 1. After calibration, these parameters were used to simulate the snow processes of the watershed.

3.2 Simulation of discharge

A simple conceptual method was used to estimate discharge according to the following equation, written for a time lag between the daily melt cycle and the resulting discharge cycle of 6 h (Martinec et al., 2005):

$$D_{n+1} = \frac{1}{2}\cdot(C_{\text{snow}}\cdot(melt_n + melt_{n+1}) + C_{\text{rain}}\cdot(rain_n + rain_{n+1}))\cdot A_l\cdot(1-k_{n+1}) + D_n k_{n+1} \quad (10)$$

where D is the average daily discharge (m^3/s), *melt* is the total snowmelt water equivalent (m), *rain* is the daily rainfall depth (m), n and $n+1$ is the sequence of days during snow season, C_{snow} is the runoff coefficient of snow, and C_{rain} is the runoff coefficient of rain. A_l is the conversion constant from mm^2/d to m^3/s. k is the recession coefficient indicating the decline of discharge in a period without snowmelt or rainfall (Martinec et al., 2005). Statistical behavior of the discharge decline in periods without snowmelt and rainfall was analyzed to obtain the recession coefficient k. Results can be formulated as

$$k_{n+1} = 0.569 \times D_n^{-0.054} \quad (11)$$

Nash and Sutcliffe efficiency statistic NSE (R^2) and volume difference Dv (%) were used to assess the accuracy of simulation results.

$$R^2 = 1 - \frac{\sum_{i=1}^{n}\left(D_i - D_i'\right)^2}{\sum_{i=1}^{n}\left(D_i - \overline{D}\right)^2} \quad (12)$$

HESSD
7, 3189–3211, 2010

$$Dv = \frac{V - V'}{V} \cdot 100 \quad (13)$$

where D_i is the daily discharge measured, D_i' is the daily discharge computed, and $\overline{D}$ is the average discharge of the simulation period measured. Dv is the percentage difference between the total runoff (%) measured and simulated, V is the seasonal runoff volume measured, and V' is the seasonal runoff volume computed.

3.3 Simulation of spatial energy inputs

3.3.1 Wind speed, air temperature, humidity, precipitation

In the model, hourly air temperatures were linearly interpolated between the two meteorological stations as a function of elevation. Wind speed values were modified according to topographic slope and curvature relationships, as Liston and Elder (2006) suggested. Relative humidity observed was converted to specific humidity, and then spatial relative humidity was extrapolated using specific humidity and previously extrapolated air temperature (Cline et al., 1998). Precipitation data were extrapolated to the altitude of each grid by an altitude gradient of about 1%, following previous observations in Binggou watershed (Yang et al., 1992). The critical temperature assumed to judge the precipitation form (snow or rain) is 1 °C.

3.3.2 Solar radiation

The total incoming solar radiation observed was separated empirically into direct and diffuse components (Bristow et al., 1985). The two components were distributed to the whole watershed.

$$\tau_d = \tau_t \cdot \left(1 - \exp\left(\frac{0.6(1 - B/\tau_t)}{B - 0.4}\right)\right) \quad (14)$$

HESSD
7, 3189–3211, 2010

where τ_d is the atmospheric diffused transmission coefficient, τ_t is the atmospheric total transmission coefficient, and B is the maximum clear sky tranmissivity of the atmosphere (0.76) (Flerchinger, 2000). τ_d is assumed to be the same over the small watershed (30.27 km^2). Complex alpine terrain modified the exchange of direct and diffused solar radiation. The incoming solar radiation on a slope can be computed according to the following equations (DeWalle and Rango, 2008):

$$S_{\text{slope}} = S_{\text{dire}} \cos Z + S_{\text{diff\_slope}} \quad (15)$$

$$S_{\text{diff\_slope}} = S_{\text{diff}}(\cos^2 k_s/2) + (1 - \cos^2 k_s/2)\alpha_t S_{\text{envi}} \quad (16)$$

where S_{slope} is the incoming shortwave radiation flux density on the slope, S_{dire} is the incoming direct shortwave radiation at normal incidence, $S_{\text{diff\_slope}}$ is the incoming diffuse shortwave radiation flux density to slope, Z is the angle between solar beam perpendicular to the slope, S_{diff} is the diffused shortwave radiation flux density on horizontal surface, k_s is the slope inclination angle, $(\cos^2 k_s/2)$, $(1 - \cos^2 k_s/2)$ represent the sky-view factor, and the fraction of the view from the slope occupied by the surrounding terrain, respectively. S_{envi} is the total shortwave radiation flux density from the surrounding terrain.

Albedo was calculated as the average of two reflectances in visible and near infrared bands. The reflectance in each band is a function of snow surface age and solar illumination angle (Dickinson et al., 1993; Tarboton, 1996). When the snow depth is less than 10 cm, the albedo is taken as the composition of ground albedo and snow surface albedo (Dickinson et al., 1993). When solar radiation entered the snowpack, the net radiation flux at different depths was calculated following the empirical equations (Anderson, 1976; Flerchinger and Cooley, 2000).

3.3.3 Longwave radiation and turbulent heat exchange

Outgoing longwave radiation was computed from the Stefan-Boltzmann equation using snow surface temperature (T_{ss}, °C). Incoming longwave radiation was estimated based

HESSD
7, 3189–3211, 2010

on air temperature (T_a, °C),

$$L_{out} = \varepsilon_s \sigma (T_{ss} + 273.16)^4 \quad (17)$$

$$L_{in} = \varepsilon_{ac} \sigma (T_a + 273.16)^4 \quad (18)$$

where ε_s is snow emissivity (0.99), ε_{ac} is air emissivity under cloudy conditions, and σ is the Stefan-Boltzmann constant ($5.67 \times 10^{-8} \mathrm{Wm^{-2}K^{-4}}$). ε_{ac} is estimated from (Bristow et al., 1985; Flerchinger, 2000),

$$\varepsilon_{ac} = (1 - 0.84C)\varepsilon_a + 0.84C \quad (19)$$

$$\varepsilon_a = 1 - a_\varepsilon \exp\left(-b_\varepsilon (T_a)^2\right) \quad (20)$$

$$C = 2.4 - 4\tau_t \quad (21)$$

where ε_a is the clear-sky air emissivity, C is the cloud cover fraction, a_ε and b_ε are empirical coefficients (Idso and Jackson, 1969), and τ_t is the atmospheric transmissivity calculated from the shortwave radiation measured. Terrain influence on incoming atmosphere longwave radiation was modified by the factors ($\cos^2 k_s/2$), ($1 - \cos^2 k_s/2$), similar to Eq. (16) (DeWalle and Rango, 2008).

The bulk aerodynamic approach was used to compute the sensible and latent heat exchange (Hood et al., 1999). Rainfall energy was also computed in the model (US Army Corps of Engineers, 1998). Ground heat conduction was assumed as a small constant value for heat flow to the snowpack.

4 Results

4.1 Daily snowcover distribution

By the linear interpolation method, daily SCF images without clouds were obtained. To prove the effectiveness of this method, the frequency of different cloudy durations in the snow season of 2008 was counted. The most frequent duration found was 1 day,

HESSD
7, 3189–3211, 2010

accounting for 53.9% of the total samples. The maximum cloudy duration was 15 days, accounting for only 0.8%, and the duration less than 4 days accounted for 91.0%. This suggests that more than half the cloudy durations were only 1 day and the rest were less than 4 days. The shorter the cloudy duration, the more reliable the interpolation results. As such, interpolation results were theoretically close to the truth.

4.2 SWE distribution and change

Spatial energy inputs are the most important factors for snowpack melting. Net energy inputs to the snowpack above the whole watershed were negative before snowmelt occurrence (Fig. 2). Shortwave radiation accounted for major parts of the total energy inputs. After 17 March, net energy inputs became positive with increasing solar radiation and air temperature. Corresponding to the changes of energy inputs, there were three marked snowmelt processes.

Total spatial SWE change at grids over the whole snow season, was calculated using SCF data calculation and energy balance method, the distribution of which has marked topographic features. SWE distribution has an increasing trend with higher altitudes. Daily snowmelt and discharge were simulated also.

5 Discussion

5.1 Validation

5.1.1 Validation by spatial samplings

There were seven field sampling regions in the Binggou watershed (A, B, D, E, F, H, I) (Fig. 1). Snow depths were sampled in these regions and the statistical results were used to validate the calculated spatial snow depth. The sampling scheme including each sampling region was divided into several sub-regions with a size of 30 m, and snow depth was sampled at each sub-region randomly. In this study, the average snow

HESSD
7, 3189–3211, 2010

depth of the total samples in each grid with a size of 60 m was counted to validate the simulated snow depth using 50 m resolution. Thirty-two snow depths were collected and averaged during March 2008 (3/11, 3/14, 3/15, 3/17, 3/19, 3/22, 3/24, 3/29, 3/30).

The simulated snow depths agreed well with the measurements in most cases (Fig. 3). The bias error (BIAS) was −2.1 cm, and Root Mean Square Error (RMSE) was 33.9 cm. Obvious errors occurred mainly in the H and I regions. These overestimated snow depths are marked in the dotted ellipse in Fig. 3. Regions I and H are located at the lower altitudes (3450 m and 3528 m, respectively) by the side of the channels in Binggou watershed. Snowpacks just begin to melt in the middle of March. For higher air temperature and increasing solar radiation, snow at lower altitudes melts faster than in other places; hence the SCA changes considerably in the H and I regions in a single day. However, there was only one MODIS image every day. In this case, the snowmelt may be overestimated because one unchanged snowcover image was used to calculate hourly snowmelt all day. The other misestimation of snow depth occurred in the B Region in 19 March. Average snow depth measured was 17.7 cm, while that of simulated snow depth was 0 cm. This occasional case was due to the snowcover existence misestimated using MODIS data.

As described above, spatial and temporal snow depth distribution can be retrieved effectively using MODIS data and energy balance method.

5.1.2 Validation of snowmelt runoff by discharge measurements

By contrasting measured and simulated discharges in snow season, total amounts and temporal trend of calculated snowmelts were validated. Daily discharges in the snow season of 2008 were computed (Fig. 4). The simulated results agreed well with the measured discharge; the NSE (R^2) was 0.673, and the volume difference Dv was 3.9%.

HESSD
7, 3189–3211, 2010

The refrozen phenomenon was not considered in computing discharge. Abundant ice bodies formed by refrozen snowmelt were found in valleys and river channels in Binggou watershed in the early spring of 2008. The thicknesses of these ice bodies varied from dozens of centimeters to a few meters. This phenomenon should have delayed the confluence of snowmelt runoff, the reason for which was quite possibly the inaccurate agreement of simulated results with the measurement obtained during the earlier snowmelt season.

5.2 Discussion of other potential errors

There are some simplified parameterization schemes in spatial energy computation. Terrain influence is an important factor in snow surface energy exchange in the alpine region. In this study, the effects of terrain on solar radiation were corrected by a simplified sky-view factor. By this method, the terrain features of solar radiation in alpine watershed could be recognized. However, the influence of surrounding terrain shading on the solar radiation was not considered in detail. Wind speed plays an important role in computing turbulent heat exchange. High-resolution wind field simulation is needed to predict snow transport and snowcover development over steep topography (Raderschall et al., 2008). Only simplified interpolation method was used in this study. For more accurate wind field simulation, other physical wind simulation model must be added. Ground heat is usually regarded as a constant in modeling snow processes (Yang, 2008), a simplification that was also used in this study. In the snow season of 2008, measured ground heat was almost a constant (10 W) in Binggou watershed. However, it changed and fluctuated with the increasing snowmelt during the later snowmelt season. Although the magnitudes of ground heat are not large relative to other heat sources such as shortwave radiation, more accurate energy exchange computation must also be considered. The spatial heterogeneity of precipitation is relatively weak in a small watershed such as Binggou; thus, only an elevation adjustment was used to correct precipitation distribution. If a larger watershed was chosen

HESSD
7, 3189–3211, 2010

to model the snow processes, the heterogeneity of precipitation should be considered in more detail.

Secondly, some elements in snow evolution processes were ignored in the computation, such as blowing snow sublimation and transport. Blowing snow sublimation plays an important role in snow hydrologic processes, and the redistribution of snowpack for interactions between blowing snow and terrain is prominent under high wind speed conditions (Pomeroy and Li, 2000). Therefore, snow sublimation may be underestimated in modeled results. On the other hand, because MODIS snowcover data were used to discriminate snowpack existence, even the redistributed snowpack can be recognized and included in calculating snowmelt. The errors from blowing snow transfer are relatively small in theory.

6 Conclusions

An energy balance method and MODIS data were used to model snow distribution and melt processes in an alpine watershed. As a result, total SWE change over the entire snow season and daily SWE distribution were obtained. Discharges were also simulated and then used to validate daily total snowmelt. Simulated snow depths were validated by field measurements. Results indicate that it is practical and relatively accurate to simulate spatial and temporal snow distribution and change using snowcover information from RS data and energy balance method.

To obtain continuous daily snowcover maps, a linear interpolation method was used. By this method, each MOD10A1 scene could be used and thus no data were wasted. Simulation results indicate that almost half of MODIS image waste could have been avoided in Binggou watershed in the snow season of 2008. With further validation and improvement, this method can be used in large-scale snowcover mapping. Using the method introduced in this article, modeling spatial snow distribution and melt runoff and removing clouds effectively will become relatively convenient.

HESSD
7, 3189–3211, 2010

Acknowledgement. This study was supported by the CAS (Chinese Academy of Sciences) Action Plan for West Development Project "Watershed Allied Telemetry Experimental Research (WATER)" (grant no: KZCX2-XB2-09), the National Natural Science Foundation of China (grant no: 40671040) and the "Coordinated Asia-European long-term Observation system of Qinghai-Tibet Plateau hydro-meteorological processes and the Asia-monsoon systEm with Ground satellite Image data and numerical Simulations" CEOP-AEGIS (Grant no.212921).

References

Bristow, K. L., Campbell, G. S., and Saxton, K. E.: An equation for separating daily solar irradiation into direct and diffuse components, Agr. Forest Meteorol., 35, 123–131, 1985.

Cline, D. W., Bales, R. C., and Dozier, J.: Estimating the spatial distribution of snow in mountain basins using remote sensing and energy balance modeling, Water Resour. Res., 34, 1275–1285, 1998.

DeWalle, D. R. and Rango, A.: Principles of Snow Hydrology, Cambridge University Press, Cambridge, 2008.

Dickinson, R. E., Kennedy, P. J., and Henderson-Sellers, A.: Biosphere-Atmosphere Transfer Scheme (BATS) version 1e as coupled to the NCAR community climate model, National Center for Atmospheric Research, Climate and Global Dynamics Division, Boulder, CO, 1993.

Durand, M., Molotch, N. P., and Margulis, S. A.: Merging complementary remote sensing datasets in the context of snow water equivalent reconstruction, Remote Sens. Environ., 112, 1212–1225, 2008.

Essery, R. and Pomeroy, J.: Implications of spatial distributions of snow mass and melt rate for snow-cover depletion: theoretical considerations, Ann. Glaciol., 38, 261–265, 2004.

Flerchinger, G. N.: The Simultaneous Heat and Water (SHAW) Model: Technical Documentation, Northwest Watershed Research Center, USDA Agricultural Research Service, Boise, ID, 2000.

Flerchinger, G. N. and Cooley, K. R.: A ten-year water balance of a mountainous semi-arid watershed, J. Hydrol., 237, 86–99, 2000.

Gafurov, A. and Bárdossy, A.: Cloud removal methodology from MODIS snow cover product, Hydrol. Earth Syst. Sci., 13, 1361–1373, doi:10.5194/hess-13-1361-2009, 2009.

HESSD

7, 3189–3211, 2010

Hall, D. K. and Riggs, G. A.: Accuracy assessment of the MODIS snow products, Newark, DE, 2006.
Hood, E., Williams, M., and Cline, D.: Sublimation from a seasonal snowpack at a continental, mid-latitude alpine site, Hydrol. Process., 13, 1781–1797, 1999.
Idso, S. B. and Jackson, R. D.: Thermal radiation from atmosphere, J. Geophys. Res., 74, 5397–5403, 1969.
Li, X., Li, X., Li, Z., Ma, M., Wang, J., Xiao, Q., Qiang, L., Che, T., Chen, E., Yan, G., Hu, Z., Zhang, L., Chu, R., Su, P., Liu, Q., Liu, S., Wang, J., Niu, Z., Chen, Y., Jin, R., Wang, W., Ran, Y., Xin, X., and Ren, H.: Watershed allied telemetry experimental research, J. Geophys. Res., 114, D22103, doi:10.1029/2008JD011590, 2009.
Liston, G. E. and Elder, K.: A meteorological distribution system for high-resolution terrestrial modeling (MicroMet), J. Hydrometeorol., 7, 217–234, 2006.
Martinec, J., Rango, A., and Roberts, R.: SRM (Snowmelt Runoff Model) User's Manual, 2005.
Painter, T. H., Rittger, K., McKenzie, C., Slaughter, P., Davis, R. E., and Dozier, J.: Retrieval of subpixel snow covered area, grain size, and albedo from MODIS, Remote Sens. Environ., 113, 868–879, 2009.
Parajka, J. and Bloeschl, G.: The value of MODIS snow cover data in validating and calibrating conceptual hydrologic models, J. Hydrol., 358, 240–258, 2008.
Pomeroy, J. W. and Li, L.: Prairie and arctic areal snow cover mass balance using a blowing snow model, J. Geophys. Res.-Atmos., 105, 26619–26634, 2000.
Raderschall, N., Lehning, M., and Schär, C.: Fine-scale modeling of the boundary layer wind field over steep topography, Water Resour. Res., 44, W09425, doi:10.1029/2007WR006544, 2008.
Seidel, K. and Martinec, J.: Remote sensing in snow hydrology: runoff modelling, effect of climate change, Springer-Praxis books in geophysical sciences, Springer; Praxis Pub., Berlin; New York, Chichester, UK, 150 pp., 2004.
Su, H., Yang, Z. L., Niu, G. Y., and Dickinson, R. E.: Enhancing the estimation of continental-scale snow water equivalent by assimilating MODIS snow cover with the ensemble Kalman filter, J. Geophys. Res.-Atmos., 113, D08120, doi:10.1029/2007jd009232, 2008.
Tarboton, D., Bloschl, G., Cooley, K., Kirnbauer, R., and Luce, C.: Spatial snow cover processes at Kuhtai and Reynolds Creek, Spatial Patterns Catchment Hydrol., 158–186, 2000.
Tarboton, D. G.: Utah Energy Balance Snow Accumulation and Melt Model (UEB), Utah Water Research Laboratory and USDA Forest Service Intermountain Research Station, 1996.

HESSD
7, 3189–3211, 2010

Tekeli, A. E., Akyurek, Z., Sorman, A. A., Sensoy, A., and Sorman, A. U.: Using MODIS snow cover maps in modeling snowmelt runoff process in the eastern part of Turkey, Remote Sens. Environ., 97, 216–230, 2005.

Yang, Z.-L., Dickinson, R. E., Robock, A., and Vinnikov, K. Y.: Validation of the snow submodel of the biosphere–atmosphere transfer scheme with Russian snow cover and meteorological observational data, J. Climate, 10, 353–373, 1997.

Yang, Z.-L.: Description of recent snow models, in: Snow and Climate: Physical Processes, Surface Energy Exchange and Modeling, edited by: Armstrong, R. L. and Brun, E., Cambridge University Press, 129–136, 2008.

Yang, Z.-N., Yang, Z.-H., and Zhang, X.-C.: Runoff and its generation model of cold region in Binggou basin of Qilian mountain (in Chinese), Memoirs of Lanzhou Institute of glaciology and geocryology, Chinese Academy of Sciences, 91–100, 1992.

Zaitchik, B. F. and Rodell, M.: Forward-looking assimilation of MODIS-derived snow-covered area into a land surface model, J. Hydrometeorol., 10, 130–148, 2009.

HESSD

7, 3189–3211, 2010

Table 1. Adjusted parameters at point scale.

Parameters	Adjusted values
New snow visible band reflectance	0.95
New snow near infrared band reflectance	0.7
Snow surface aerodynamic roughness	0.0001 m
Snow emissivity	0.98
The maximum liquid-water-retaining fraction of snowpack	5%
Snow density	260 kg/m^3
Ground heat	10 W
Bare soil albedo	0.26
Critical temperature of precipitation forms (snow OR rain)	1 $^\circ$C

HESSD
7, 3189–3211, 2010

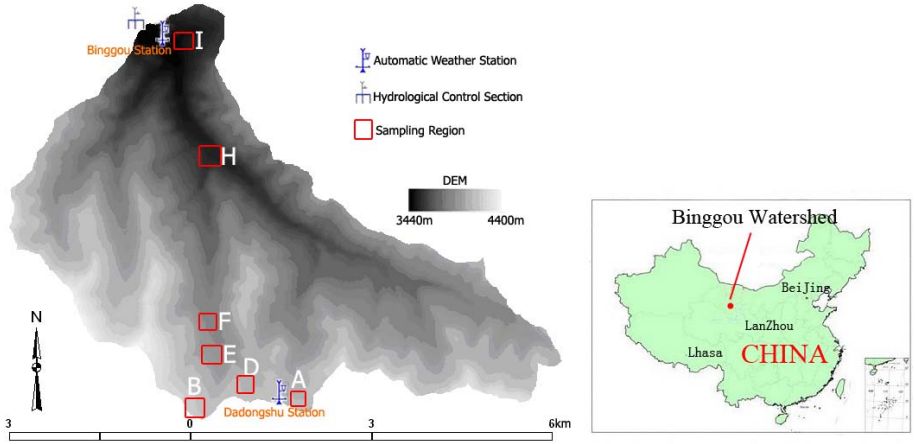

Fig. 1. Map of the Binggou watershed.

HESSD
7, 3189–3211, 2010

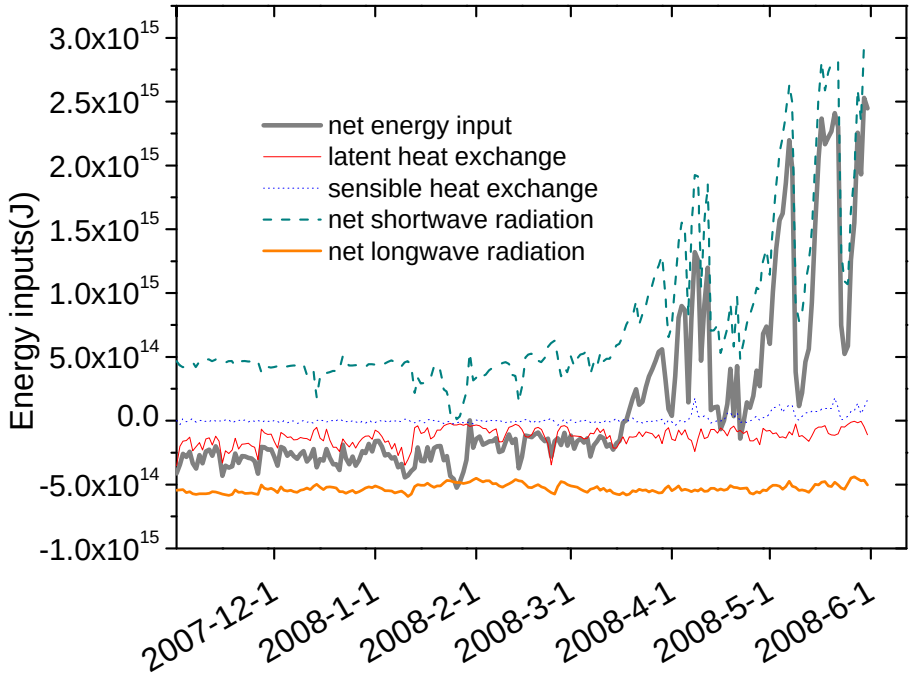

Fig. 2. Different daily energy inputs to snowpack of the total watershed in 2008 snow season.

HESSD
7, 3189–3211, 2010

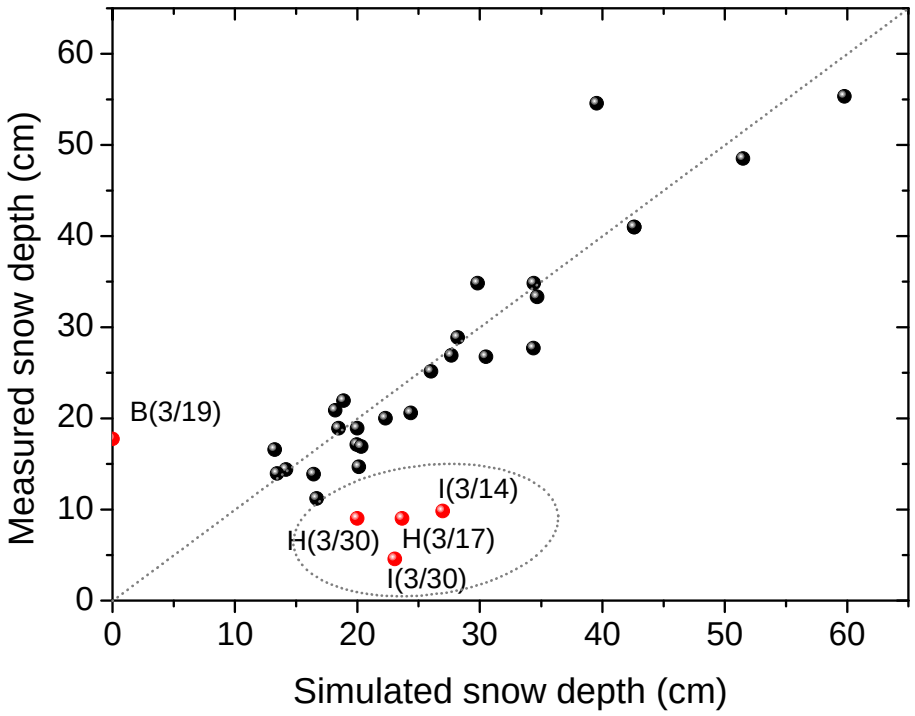

Fig. 3. Validation of simulated snow depths using measured snow depths at sampling regions in Binggou watershed (H(3/30) represents measured snow depth at H region in 30 March, and so on).

HESSD
7, 3189–3211, 2010

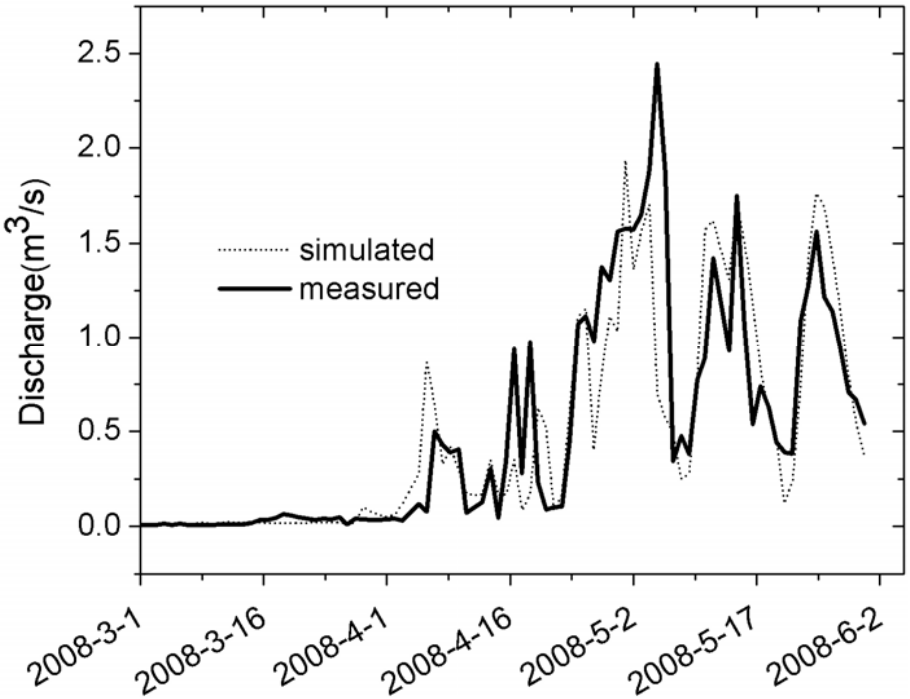

Fig. 4. Contrast between simulated and measured discharges.

HESSD
7, 3189–3211, 2010